

Learning Theory for Estimation of Animal Motion Submanifolds

Nathan Powell

Department of Mechanical Engineering
Virginia Tech
Blacksburg, Virginia, USA
nppowell@vt.edu

Andrew J. Kurdila

Department of Mechanical Engineering
Virginia Tech
Blacksburg, Virginia, USA
kurdila@vt.edu

Abstract—This paper describes the formulation and experimental testing of a novel method for the estimation and approximation of submanifold models of animal motion. It is assumed that the animal motion is supported on a configuration manifold Q that is a smooth, connected, regularly embedded Riemannian submanifold of Euclidean space $X \approx \mathbb{R}^d$ for some $d > 0$, and that the manifold Q is homeomorphic to a known smooth, Riemannian manifold S . Estimation of the manifold is achieved by finding an unknown mapping $\gamma : S \rightarrow Q \subset X$ that maps the manifold S into Q . The overall problem is cast as a distribution-free learning problem over the manifold of measurements $\mathbb{Z} = S \times X$. That is, it is assumed that experiments generate a finite sets $\{(s_i, x_i)\}_{i=1}^m \subset \mathbb{Z}^m$ of samples that are generated according to an unknown probability density μ on \mathbb{Z} . This paper derives approximations $\gamma_{n,m}$ of γ that are based on the m samples and are contained in an $N(n)$ dimensional space of approximants. The paper defines sufficient conditions that shows that the rates of convergence in $L^2_\mu(S)$ correspond to those known for classical distribution-free learning theory over Euclidean space. Specifically, the paper derives sufficient conditions that guarantee rates of convergence that have the form

$$\mathbb{E} \left(\|\gamma_\mu^j - \gamma_{n,m}^j\|_{L^2_\mu(S)}^2 \right) \leq C_1 N(n)^{-r} + C_2 \frac{N(n) \log(N(n))}{m}$$

for constants C_1, C_2 with $\gamma_\mu := \{\gamma_\mu^1, \dots, \gamma_\mu^d\}$ the regressor function $\gamma_\mu : S \rightarrow Q \subset X$ and $\gamma_{n,m} := \{\gamma_{n,m}^1, \dots, \gamma_{n,m}^d\}$.

Index Terms—learning theory, animal motion, estimation, bioinspiration

I. INTRODUCTION

The related problems of understanding the underlying dynamics of animal locomotion, constructing (multibody) dynamics models of animals, or building robots that emulate animals has occupied researchers having diverse backgrounds. References [1]–[27], [27]–[38] are representative of the breadth of research in these related fields. This class of research includes investigations related to, or based upon, the motions of humans, bats, birds, lizards, geckos, sheep, frogs, beetles, and cheetahs [8], [11], [12], [17], [27]. Some studies such as in [7], [34], [35] seek to understand the underlying geometry of the mechanics of human or other animal motion. Others are expressly interested in the construction of low dimensional models of complex motion [25], [26]. Some are dedicated to finding how qualitative understandings of animal motion can be used to build robots that emulate some

observed motion [5], [9]. A fundamental question that is either motivated or directly addressed by these studies is how to come up with a general method for defining a principled, low-dimensional model of a complex animal motion. The aim of our research is to provide further insight into the motion of animals by deriving a general method to discover and approximate an underlying manifold on which the dynamics evolves.

Historically, the theory that has been used to derive models of animal motion have been around for some time. Multibody dynamics formulations [39]–[41], [41] derived in terms of analytical mechanics are well-known, and constitute the foundation of general simulation packages like MSC Adams®, OpenSim®, Solidworks®, and NX®. These approaches give rise to models that allow for rigid or flexible bodies, linear or nonlinear deformation models of individual bodies, and either ideal or more general types of constraints among bodies. See the references in [39] for a good overview. While the use of analytical mechanics as the basis of such formulations can be traced back several decades, one recent trend in the field of multibody dynamics has been the study of geometric methods based on manifolds and differential geometry. [42]–[44] It is fair to say that while such differential-geometric descriptions are couched in a language that is substantially more rigorous than the older approaches derived from analytical mechanics, the latter have given rise to a wider class of models that are now commonly used for more general systems. Most of the recent expositions such as [42]–[44] that overview geometric methods for multibody systems assume that the constituent bodies are rigid and constraints are ideal. While in principle much more complex multibody systems could be attacked using geometric methods, the rigor of the formulation inhibits easy extension to some of the classes of problems that have been modeled via (the field formerly known as) analytical mechanics. We note that, at least so far to the authors knowledge, the use of geometric methods for multibody systems have not reached the level of abstraction as the geometric methods in [45], [46] where the states spaces are infinite dimensional manifolds required to describe flexible bodies.

As discussed carefully in [44], one of the primary theoretical advantages of geometric method is their abstraction: states of the system are known to be elements of manifolds, which are

by their nature coordinate-free. This generality is particularly attractive in the problem at hand. Intuitively, we want to approximate or identify some “lower-dimensional mathematical object” that underlies an observed motion of a complex, higher order multibody system. We want to ensure that any associated algorithm converges to a coordinate independent entity. In this paper we introduce the analysis and experimental testing of a method to identify and approximate motions over a *finite dimensional* submanifold that underlies a particular motion regime observed during animal motion. We work to formulate the problem in such a way that we can guarantee that approximations converge, in some appropriate sense, over the underlying manifold.

We begin in Section II-B with a careful description of the problem of estimating a motion manifold as one of distribution-free learning over manifolds. This problem is substantially more complicated than the conventional problems for functions defined over Euclidean spaces. This new learning problem is made complex in no small part owing to the difficulty of in defining appropriate function spaces and spaces of approximants over manifolds. These two topics are covered in Sections II-C and II-D, respectively. In particular, we introduce the linear approximation spaces $A^{r,2}(L_\mu^2(S))$ for a smooth manifold S , and these play a crucial role in deriving rates of convergence. The primary theoretical result of this paper gives sufficient conditions to ensure that approximations $\gamma_{n,m} : S \rightarrow X$ of the unknown function $\gamma : S \rightarrow Q \subset X$ converge to the regressor function $\gamma_\mu : S \rightarrow X$. We show that when the regressor function satisfies the smoothness condition $\gamma_\mu \in (A^{r,2}(L_\mu^2(S)))^d$, the rate of convergence is given by

$$\mathbb{E}(\|\gamma_\mu^j - \gamma_{n,m}^j\|_{L_\mu^2}) \leq C_1(N(n))^{-r} + C_2 \frac{N(n) \log(N(n))}{m} \quad (1)$$

for constants $C_1, C_2 > 0$, where $\mathbb{E}(\cdot)$ is the expectation over samples, $N(n)$ is the dimension of the space of approximants, and m is the number of samples. This is precisely the rate achieved for certain approximations of distribution-free learning problems over Euclidean space. Such rates of convergence are known to be optimal, except for the logarithmic factor. [47] Finally, this paper concludes in Section III with a study of the performance of the proposed method using samples from recent reptile motion studies.

II. PROBLEM FORMULATION

A. Kinematics and Inherent Geometry

For purposes of ensuring convergence of approximations, we assume in this paper that motions are contained in the ambient space $X \approx \mathbb{R}^d$ for some $d > 0$. Of course this space suffices to describe the dynamics of multibody systems comprised of assemblies of lumped masses where motion is specified in terms of the mass centers of the (inertia-free) bodies. Since in principle any Riemannian manifold can be (isometrically) embedded in \mathbb{R}^d via the Nash embedding theorem, in principle this assumption also allows for some of the other standard models where the configuration manifold includes $SO(3)$ or $SE(3)$ as described in [?]. It is assumed

that the motion of the system is supported on a smooth, compact, connected, Riemannian manifold Q that is a regularly embedded in the ambient space X . This manifold is taken to be homeomorphic to some smooth manifold S . We denote the homeomorphism by $\gamma : S \rightarrow Q$ where $\gamma := [\gamma^1, \dots, \gamma^d]^T$ and $\gamma^i : S \rightarrow \mathbb{R}$, and we discuss its smoothness in our discussion of approximation spaces in Section II-C. The manifold S is equipped with the topology induced by its intrinsic Riemannian metric and Q is equipped with the topology inherited as a regularly embedded submanifold $Q \subseteq X \approx \mathbb{R}^d$.

B. The Distribution-Free Learning Problem on Manifolds

This paper is concerned with finding the mapping γ that determines the low-dimensional underlying manifold Q that supports a given motion or motion regime. We choose to formulate this problem as one of *distribution-free* learning theory on manifolds. In distribution-free learning theory it is assumed that we are given a collection of independent and identically distributed samples $\{z_i\}_{i=1}^m := \{(s_i, q_i)\}_{i=1}^m \subset \mathbb{Z} := S \times X$ that are generated by some *unknown* probability measure μ on the space \mathbb{Z} . In order to determine the mapping from the known manifold S to the configuration space Q , it would be ideal if we could determine an optimal mapping $\hat{\gamma} : S \rightarrow Q \subset X$ such that

$$\hat{\gamma} = \arg \min_{\gamma \in \Gamma} E_\mu(\gamma) := \arg \min_{\gamma \in \Gamma} \int_{\mathbb{Z}} \|\gamma - \gamma(s)\|_X^2 \mu(dz) \quad (2)$$

where $z = (s, q) \in \mathbb{Z}$ and Γ is a set of admissible operators that map from $S \rightarrow Q$. Solving the optimization problem 2 poses a number of difficulties, some of which are rather standard challenges in the field of distribution-free learning theory. For example, it is well-known that the ideal solution $\hat{\gamma}$ above cannot be computed from the minimization problem in Equation 2 since the measure μ on \mathbb{Z} is unknown. For this reason methods of empirical risk minimization are used that substitute a discrete proxy for the expression in Equation 2. We discuss this step in detail shortly in Section II-E.

Beyond these conventional challenges to building approximations of $\hat{\gamma}$, there are additional substantial difficulties that are unique to the problem at hand. In classical treatments of distribution-free learning theory, the rates of convergence of approximations to the solution are often cast in terms of approximation spaces or smoothness spaces (that often end up being Sobolev spaces) of real-valued functions over subsets of Euclidean space \mathbb{R}^p . That is, the space Γ is usually selected to be some subset of the real-valued functions over subsets of Euclidean space. Here, however, the functions $\gamma \in \Gamma$ are mappings from the manifold S to the manifold $Q \subset X$. The definition of Sobolev mappings between manifolds is a complicated subject, and for general choices of S or Q it is unclear exactly what definition of smoothness should be selected. A significant part of this paper is dedicated to defining approximation spaces over manifolds and subsequently structuring the learning problem so convergence results can be derived in a way that is analogous to the classical case over subsets of Euclidean Space.

C. Function Spaces on Manifolds

In the setup of the problem above we have assumed that S is a known, compact, connected, smooth Riemannian manifold, and that Q is a regularly embedded submanifold of $X := \mathbb{R}^d$. This means that the unknown function $\gamma : S \rightarrow Q$ is constructed of component functions $\gamma^i : S \rightarrow \mathbb{R}$ for $i = 1, \dots, d$. In this section we define the various function spaces over manifolds that will be used to approximate the functions γ^i . The function spaces over the manifolds S , Q or X that are used in this paper consist of certain spaces of square-integrable functions and native spaces of a reproducing kernel. When μ_S is a measure over the manifold S , the usual space of real-valued, μ_S -square integrable functions is given by $L_\mu^2 := L_{\mu_S}^2(S)$, which is a Hilbert space with respect to the usual inner product $(f, g)_{L_\mu^2} := \int_S f(\xi)g(\xi)\mu_S(d\xi)$. Recall [48], [49] that a real RKH space \mathbb{H}^A over an arbitrary set A is defined to be

$$\mathbb{H}^A := \overline{\text{span} \{k_a^A \mid a \in A\}}$$

where $k_a^A := k^A(a, \cdot)$ and $k^A : A \times A \rightarrow \mathbb{R}$ is a real, positive semi-definite, symmetric, continuous admissible kernel function. This definition of an RKH space makes sense over a general set A , and in particular makes sense for the specification of functions over manifolds. We denote by $k^X : X \times X \rightarrow \mathbb{R}$ the kernel of the RKH Space \mathbb{H}^X over the set X . The restriction of functions in \mathbb{H}^X to the set Q always defines an RKH space over Q , and we set

$$\mathbb{H}^Q := \left\{ g|_Q \mid g \in \mathbb{H}^X \right\}.$$

The kernel $k^Q : Q \times Q \rightarrow \mathbb{R}$ that defines the space of restrictions \mathbb{H}^Q is given by

$$k^Q(x, y) := k^X(x, y) \Big|_Q, \quad \forall x, y \in Q,$$

which is a classical result from the theory of RKH spaces. Finally, we define the pullback space $\mathbb{H}^S := \gamma(\mathbb{H}^Q)$ on S as

$$\gamma^S(\mathbb{H}^Q) := \{ g \circ \gamma \mid g \in \mathbb{H}^Q \},$$

and the kernel k^S defined on the manifold S is written as

$$k^S(\alpha, \beta) = k^Q(\gamma(\alpha), \gamma(\beta)).$$

D. Approximant Spaces

The approximations in this paper are constructed in terms of two different types of finite dimensional spaces of approximants.

1) *Approximants in $L_\mu^2(S)$* : When we build approximations in $L_\mu^2(S)$, we make use of a nested sequence $\{\mathcal{S}_n\}_{n=1}^\infty$ of measurable partitions \mathcal{S}_n of S , where each partition $\mathcal{S}_n := \{S_{n,k}\}_{k=1}^{N(n)}$. That is, these sets satisfy $S = \bigcup_{k=1}^{N(n)} S_{n,k}$, $S_{n,k} \cap S_{n,\ell} = \emptyset$ for all $\ell \neq k$, and $S_{n,k} = \bigcup_{\ell \in \Lambda_{n,k}} S_{n+1,\ell}$ for some finite set of indices $\Lambda_{n,k}$. Here $N(n) = \#(\mathcal{S}_n)$ is the number of sets in the n^{th} partition \mathcal{S}_n . We define the space

of approximants \mathbb{H}_n^S as the span of the characteristic functions $1_{S_{n,k}}$ of the sets in \mathcal{S}_n ,

$$\mathbb{H}_n^S := \text{span}\{1_{S_{n,k}} \mid 1 \leq k \leq N(n)\} \subset L_\mu^2(S) \quad (3)$$

where $\{1_{S_{n,k}}\}_{k=1}^{N(n)}$ is the associated partition of unity over S . We associate to the partition \mathcal{S}_n a set of representatives,

$$\Xi_n := \{\xi_{n,k} \mid \xi_k \in S_{n,k}, k = 1, \dots, N(n)\},$$

These representative points are assumed to fill the manifold in the sense that the fill distance

$$h_{\Xi_n, S} := \max_{s \in S} \min_{\xi_{n,k} \in \Xi_n} d(s, \xi_{n,k}) \rightarrow 0$$

as $n \rightarrow \infty$. For any $g \in L_\mu^2(S)$ we define the L_μ^2 -orthogonal projection Π_n^S in the usual way,

$$\begin{aligned} \Pi_n^S g(\cdot) &= \sum_{k=1}^{N(n)} \int_{S_{n,k}} g(x) \frac{1_{S_k}(s)\mu_S(ds)}{\sqrt{\mu_S(S_{n,k})}} \frac{1_{S_{n,k}}(\cdot)}{\sqrt{\mu_S(S_{n,k})}}, \\ &= \sum_{k=1}^{N(n)} \frac{\int_{S_{n,k}} g(x)\mu_S(ds)}{\mu_S(S_{n,k})} 1_{S_{n,k}}(\cdot). \end{aligned}$$

We define the linear approximation space $A^{r,2}(L_\mu^2) \subseteq L_\mu^2(S)$ as

$$A^{r,2}(L_\mu^2) := \left\{ g \in L_\mu^2(S) \mid \exists C \text{ s.t. } \|(I - \Pi_n^S)g\|_{L_\mu^2} \leq C(N(n))^{-r} \right\}$$

The infimum of the constants C for which in the inequality above holds defines a semi-norm on $A^{r,2}(L_\mu^2)$.

2) *Approximants in \mathbb{H}^S* : Approximations are also constructed in terms the finite dimensional spaces of approximants

$$\begin{aligned} \mathbb{H}_m^S &:= \text{span}\{k_{s_i}^S \mid 1 \leq i \leq m\} \subset \mathbb{H}^S \\ \mathbb{H}_m^Q &:= \text{span}\{k_{s_i}^Q \mid 1 \leq i \leq m\} \subset \mathbb{H}^Q, \end{aligned}$$

that are defined in terms of the samples $\{(s_i, x_i)\}_{i=1}^m \subset \mathbb{Z}$.

E. Empirical Risk Minimization over Manifolds

As noted above, in some ideal sense the optimal choice of the mapping $\gamma : S \rightarrow Q$ is the one that extremizes the cost functional E_μ in Equation 2. Since the measure μ that generates the samples in \mathbb{Z} is unknown, distribution-free learning theory uses a proxy that can be computed to re-cast the optimization problem. The form of the empirical risk can best be motivated by first rewriting the ideal risk E_μ in terms of the regressor function. Any measure μ on the space of samples \mathbb{Z} can be rewritten (disintegrated) into the expression $\mu(dz) := \mu(dx|s) \mu_S(ds)$ with $z := (s, x)$, μ_S the associated marginal measure over S , and $\mu(\cdot|s)$ the conditional probability measure on X given $s \in S$. From first principles it is straightforward to show that we can rewrite the ideal cost E_μ in the alternative form

$$E_\mu(\gamma) = \int_S \|\gamma(s) - \gamma_\mu(s)\|^2 \mu_S(ds) + E_\mu(\gamma_\mu) \quad (4)$$

where

$$\gamma_\mu(s) := \int_X x \mu(dx|s)$$

is the regressor function associated with the measure $\mu(dz) := \mu(dx|s)\mu_X(ds)$. This decomposition shows, in fact, that the optimal mapping $\hat{\gamma}$ that minimizes $E_\mu(\gamma)$ is the regressor function $\hat{\gamma} := \gamma_\mu$. Since the last term on the right in Equation 4 is a constant that does not depend on γ , we introduce the empirical risk

$$E_m(\gamma) = \frac{1}{m} \sum_{i=1}^m \|x_i - \gamma(s_i)\|_X^2 \quad (5)$$

in terms of the samples $\{(s_i, x_i)\}_{i=1}^m \subset \mathbb{Z}$. Note that the cost functional $E_m(\gamma)$ can be computed for any admissible function γ since the samples are known. We will be interested in two types of approximations of the empirical risk in the discussions that follow. We define

$$\gamma_{n,m} = \arg \min_{\gamma_n \in H_n^S} \frac{1}{m} \sum_{i=1}^m \|x_i - \gamma_n(s_i)\|_X^2 \quad (6)$$

when we seek approximations that converge in L_μ^2 . This definition has the advantage that it is possible to derive strong convergence rates for the approximations $\gamma_{n,m} \rightarrow \gamma_\mu$. However, the resulting approximations are not very smooth. Alternatively, we set

$$\gamma_{n,m} = \arg \min_{\gamma_n \in \mathbb{H}_n^S} \frac{1}{m} \sum_{i=1}^m \|x_i - \gamma_n(s_i)\|_X^2 \quad (7)$$

when we seek smoother representations of the mapping $\gamma_{n,m}$. As of yet, we have not derived such strong rates of convergence $\gamma_{n,m} \rightarrow \gamma_\mu$ in this case. However, numerical examples compare the performance of the estimates in 6 and 7.

Before we study the solutions of these distribution-free learning problems over the manifold S , we make one last observation regarding the form of minimization problem. By introducing the samples $x_i := \{x_i^1, \dots, x_i^d\}^T$ and mapping $\gamma_n := \{\gamma_n^1, \dots, \gamma_n^d\}^T$, we can write

$$\begin{aligned} \gamma_{n,m} &= \arg \min_{\gamma_n \in H_n^S} \frac{1}{m} \sum_{i=1}^m \sum_{j=1}^d (x_i^j - \gamma_n^j(s_i))^2 \\ &= \arg \min_{\gamma_n \in H_n^S} \sum_{j=1}^d E_m^j(\gamma_n^j) \end{aligned}$$

with $E_m^j(\gamma_n^j) := \frac{1}{m} \sum_{i=1, \dots, m} (x_i^j - \gamma_n^j(s_i))^2$. Note that since each term $E_m^j(\gamma_n^j)$ is positive, the optimal $\gamma_{n,m}$ can be obtained by extremizing each of the terms $E_m^j(\gamma_n^j)$ for the component functions γ_n^j for $j = 1, \dots, d$. The primary theoretical result of this paper is summarized in the following theorem, which shows the distribution free learning problem over manifold S

Theorem 1: The optimal solution $\gamma_{n,m} := [\gamma_{n,m}^1, \dots, \gamma_{n,m}^d]^T$ of the empirical risk minimization problem in Equation 5 is given by

$$\gamma_{n,m}^j(s) = \sum_{k=1}^n \frac{\sum_{i=1}^m 1_{S_k}(s) x_i^j}{\sum_{i=1}^m 1_{S_k}(s)} 1_{S_k}(s).$$

If the regressor $\gamma_\mu \in A^{r,2}(L_\mu^2(S))$, we have the error bound

$$\mathbb{E}(\|\gamma_\mu^j - \gamma_{n,m}^j\|_{L_\mu^2}) \leq C_1(N(n))^{-r} + C_2 \frac{N(n) \log(N(n))}{m} \quad (8)$$

where the constant C_1 is independent of γ and $C_2 = C_2(\gamma)$ and $\mathbb{E}(\cdot)$ is the expectation on S^m with the product measure μ_S^m .

Proof: When we define $\gamma_n^j := \sum_{k=1, \dots, n} \hat{\alpha}_{n,k}^j 1_{S_k}(\cdot)$, we have the explicit representation of $E_m^j(\gamma_n^j)$ given by

$$E_m^j(\gamma_n^j) = \frac{1}{m} \sum_{i=1}^m \left(x_i^j - \sum_{k=1}^n \hat{\alpha}_{n,k}^j 1_{S_k}(s_i) \right)^2.$$

We can also write this sum as

$$E_m^j(\gamma_n^j) = \frac{1}{m} \sum_{k=1}^n \sum_{i=1}^m \left(1_{S_k}(s_i) x_i^j - \hat{\alpha}_{n,k}^j 1_{S_k}(s_i) \right)^2,$$

and this summation can be reordered as

$$E_m^j(\gamma_n^j) = \frac{1}{m} \sum_{k=1}^n E_{m,n}^j(\hat{\alpha}_{n,k}^j)$$

$$E_{m,n}^j(\hat{\alpha}_{n,k}^j) = \sum_{i=1}^m (1_{S_k}(s_i) x_i^j - \hat{\alpha}_{n,k}^j 1_{S_k}(s_i))^2$$

with each $E_{m,n}^j(\hat{\alpha}_{n,k}^j)$ depending on a single variable $\hat{\alpha}_{n,k}^j$. By taking the partial derivative $\partial(E_{m,n}^j(\hat{\alpha}_{n,k}^j)) = 0$, we see that

$$\hat{\alpha}_{n,k}^j = \frac{\sum_{i=1}^m 1_{S_k}(s_i) x_i^j}{\sum_{i=1}^m 1_{S_k}(s_i)},$$

which establishes the form of solution stated above. We now turn to the consideration of the error bound in the theorem. From the triangle inequality

$$\|\gamma_\mu - \gamma_{n,m}\|_{L_\mu^2} \leq \|\gamma_\mu - \Pi_n^S \gamma_\mu\|_{L_\mu^2} + \|\Pi_n^S \gamma_\mu - \gamma_{n,m}\|_{L_\mu^2}$$

we can bound the first term above by $(N(n))^{-r}$ from the definition of the linear approximation space $A^{r,2}(L_\mu^2(S))$. The bound in the theorem is proven if we can show that there is a constant C_2 such that $\|\Pi_n^S \gamma_\mu^j - \gamma_{n,m}\|_{L_\mu^2(S)} \leq C_2 N(n) \log(N(n))/m$. We establish this bound by a straightforward extension to functions on the manifold S of the proof in [50], which is given for functions defined on \mathbb{R}^p for $p \geq 1$. The expression above for $\gamma_{n,m}^j$ can be written in the form $\gamma_{n,m}^j := \sum_{k=1}^{N(n)} \alpha_{n,k}^j 1_{S_{n,k}}$, and that for $\Pi_n^S \gamma_\mu^j$ can be written as $\gamma_\mu^j := \sum_{k=1}^{N(n)} \hat{\alpha}_{n,k}^j 1_{S_{n,k}}$. In terms of these expansions, we write the error as

$$\|\Pi_n^S \gamma_\mu^j - \gamma_{n,m}\|_{L_\mu^2(S)}^2 = \sum_{k=1}^{N(n)} \left(\alpha_{n,k}^j - \hat{\alpha}_{n,k}^j \right)^2 \mu_S(S_{n,k})$$

Let $\epsilon > 0$ be an arbitrary, but fixed, positive number. We define the set of indices $\mathcal{I}(\epsilon)$ that denote subsets $S_{n,k}$ that have, in a sense, small measure,

$$\mathcal{I}(\epsilon) := \left\{ k \in \{1, \dots, N(n)\} \mid \mu_S(S_{n,k}) \leq \frac{1}{8N(n)\bar{X}^2} \right\}$$

where \bar{X} is $\sup_{s \in S} \|\gamma(s)\|_X$. We define the complement $\bar{\mathcal{I}}(\epsilon) := \{k \in \{1 \dots N(n)\} \mid k \notin \mathcal{I}\}$, and then set the associated sums

$S_I := \sum_{k \in I} (\alpha_{n,k}^j - \hat{\alpha}_{n,k}^j)^2 \mu_S(S_{n,k})$ and $S_{\tilde{I}} := \sum_{k \in \tilde{I}} (\alpha_{n,k}^j - \hat{\alpha}_{n,k}^j)^2 \mu_S(S_{n,k})$. The bound in Equation 8 follows if we can demonstrate a concentration of measure formula

$$\begin{aligned} \text{Prob} \left(\|\Pi_n^S \gamma_\mu^j - \gamma_{n,m}^j\|_{L_\mu^2}^2 > \epsilon^2 \right) \\ = \text{Prob}(S_I + S_{\tilde{I}} > \epsilon^2) \leq b e^{c m \epsilon^2 / N(n)} \end{aligned} \quad (9)$$

for some constants b, c . See [47], [50] for a discussion of such concentration inequalities. The fact that such a concentration inequality implies the bound in expectation in Equation 8 is proven in [50] on page 1311 for functions over Euclidean space. The argument proceeds exactly in the same way for the problem at hand by integration of the distribution function defined by Equation 9 over the manifold S . To establish the concentration inequality, let us define two events

$$\begin{aligned} E_{I+\tilde{I}}(\epsilon) &:= \{z \in \mathbb{Z}^m \mid S_I + S_{\tilde{I}} \geq \epsilon^2\} \\ E_{\tilde{I}}(\epsilon) &:= \left\{ z \in \mathbb{Z}^m \mid S_{\tilde{I}} \geq \frac{1}{2} \epsilon^2 \right\} \end{aligned}$$

We can compute directly from the definitions of the coefficients $\alpha_{n,k}^j, \hat{\alpha}_{n,k}^j$, and using the compactness of $\gamma(S) \subset X$, that $S_I \leq \epsilon^2/2$ for any $\epsilon > 0$. Since we always have

$$\begin{aligned} \sum_{k \in \tilde{I}} \left(\alpha_{n,k}^j - \hat{\alpha}_{n,k}^j \right)^2 \mu_S(S_{n,k}) \\ > \epsilon^2 - \sum_{k \in I} \left(\alpha_{n,k}^j - \hat{\alpha}_{n,k}^j \right)^2 \mu_S(S_{n,k}) > \frac{1}{2} \epsilon^2, \end{aligned}$$

we know that $E_{I+\tilde{I}}(\epsilon) \subseteq E_{\tilde{I}}(\epsilon)$ for any $\epsilon > 0$. If the inequality $S_{\tilde{I}} > \epsilon^2/2$, then we know there is at least one $\tilde{k} \in \tilde{I}$ such that

$$S_{\tilde{k}}(\epsilon) := (\alpha_{n,k}^j - \hat{\alpha}_{n,k}^j)^2 \mu_S(S_{n,k}) > \frac{1}{2\#\tilde{I}} \epsilon^2 > \frac{1}{2N(\epsilon)} \epsilon^2.$$

When we define the event $E_k(\epsilon) := \{z \in \mathbb{Z}^m \mid S_k(\epsilon) > \epsilon^2/2N(n)\}$ for each $k \in \{1, \dots, N(n)\}$, we conclude

$$E_{I+\tilde{I}} \subseteq E_{\tilde{I}}(\epsilon) \subseteq \bigcup_{k \in \tilde{I}} E_k.$$

By the monotonicity of measures, we conclude that $\text{Prob}(I + \tilde{I}) \leq \sum_{k \in \tilde{I}} \text{Prob}(E_k)$. But we can show, again by a simple modification of the arguments on page of [50], that $\text{Prob}(E_k) \leq e^{-c m \epsilon^2 / N(n)}$. The analysis proceeds as in that reference by using Bernsteins inequality for random variables defined over the probability space (S, Σ_S, μ_S) instead of over Euclidean space.

III. EXPERIMENTS AND NUMERICAL EXAMPLES

A number of experiments and simulations have been carried out to study the performance of the analysis in the paper. Photoreflective markers were placed on specimens of *anolis sagrei* as depicted in Figure 1, which then traversed an inclined, narrow board within the line of sight of three high speed, Photron FASTCAM @cameras. Video imagery was recorded at 500 fps, and inertial estimates of the markers were estimated using the publically distributed software toolbox [51]. The motion of a total of 21 lizards were recorded, of which 15

were male and the remaining 6 were female. Figure 2 depicts one set of inertial trajectories for the markers on the lizard. Details of the experimental setup, experimental parameters, specimen measurements, and image processing details can be found in [?].



Fig. 1: Specimen *anolis sagrei* with markers.

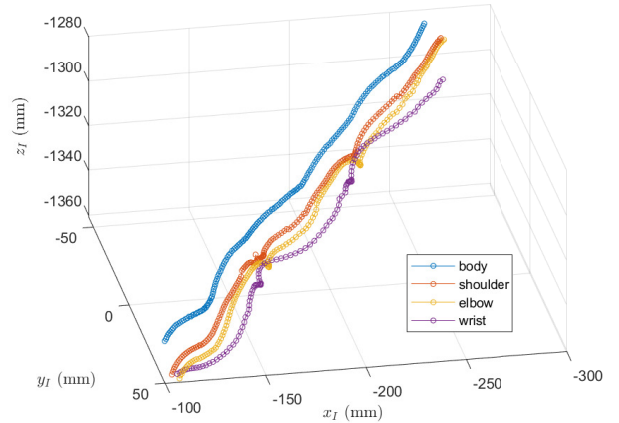


Fig. 2: Inertial Trajectories of the markers placed on a lizard in three-dimensional space.

The discrete inertial trajectories are interpreted as measured samples $\{(t_i, x_i)\}_{i=1}^m \subset [0, \infty) \times X$. In this example we choose the known manifold $S = S^1$, the circle in \mathbb{R}^2 . A post-processing step identifies a gait period T_p by inspection of the video. Using linear interpolation over each interval $[t_p, t_p + T_p]$, we can determine the s_i corresponding to the i^{th} discrete time t_i as

$$s_i = \frac{t_i - t_p}{T_p}$$

This process allows us to map the time-dependent samples $\{(t_i, x_i)\}_{i=1}^m$ to samples $\{(s_i, x_i)\}_{i=1}^m \subset S \times X = \mathbb{Z}$. The latter samples are used to build the solution of the the empirical risk minimization problem.

The approximate estimate $\gamma_{n,m}$ is obtained as the solution of the empirical risk minimization problem for two choices of approximant subspaces in the plots that follow. The first method over H_n^S carries out the minimization in terms of the characteristic functions $1_{S_{n,k}}$ defined over the partition \mathcal{S}_n of the manifold S^1 . Thus, in all the plots, the solutions obtained by minimization over H_n^S are examples of the method studied in this paper. The second method performs the minimization over \mathbb{H}_n^S and solves for $\gamma_{n,m}$ in terms of the exponential kernel basis. This method is not studied in this paper, but is included for comparison of the qualitative nature of the solution. The solution over \mathbb{H}_n^S has been computed via the EDMD algorithm using the subspaces \mathbb{H}_n^S defined in Section II-D. [52] The centers of the basis that defines \mathbb{H}_n^S are given by the centers of the partition $S_{n,k}$ used in H_n^S . Figure 3 illustrates the approximants $\gamma_{n,m}^j$ for a fixed $j \in \{1, \dots, d\}$ generated from the various two methods over the low dimensional manifold S embedded in the plane of \mathbb{R}^2 using 32 centers for both methods. In the figure, the x_i of the sample (s_i, x_i) are depicted as scattered data over one gait period. It is not clear (even qualitatively) from the simulations if the approximation obtained by the EDMD algorithm *using a smooth kernel basis for \mathbb{H}_n^S* converges to the solution obtained in this paper via empirical risk minimization over the manifold S . It has been shown in [53] that if the basis for the EDMD is selected to be the same as the characteristic functions that are in H_n^S , then the EDMD method reduces to the solution obtained via empirical risk. But the proof there relied upon particular properties

In this study, we also have performed families of simulations to illustrate convergence with respect to the numbers of centers. Figure 4 illustrates the effects that the number of centers has on the fidelity of the approximation. For both methods, it is clear that increasing the dimension number n of partitions corresponds to a higher resolution that manages to capture changes in the data over smaller intervals. Since we do not have an analytic expression for the unknown mapping γ in this actual experiment, it is impossible to verify rates of convergence directly. We leave this study to future research that uses analytic data instead of actual experimental observations.

The approximations generated from the exponential kernel given by $k_\xi(s) = e^{-\beta \|\xi - s\|^2}$ are also dependent on the hyperparameter β . Figure 5 illustrates the effects of the hyperparameter β on the approximation. For an exponential basis, larger values of β result in basis function that decay rapidly from the center, "sharpening" the curve. This results in a more oscillatory approximation from the basis functions. Thus, while the optimization of the empirical risk for functions in H_n^S yields nonsmooth estimates, there is no analog to the hyperparameter β . Depending on the hyperparameter β , highly oscillatory solutions can result for different choices of β even, even for EDMD solutions over approximant spaces

having the same dimension $N(n)$. Such oscillations can be addressed in the EDMD methods or Gaussian process models by introducing a regularization parameter. [52]

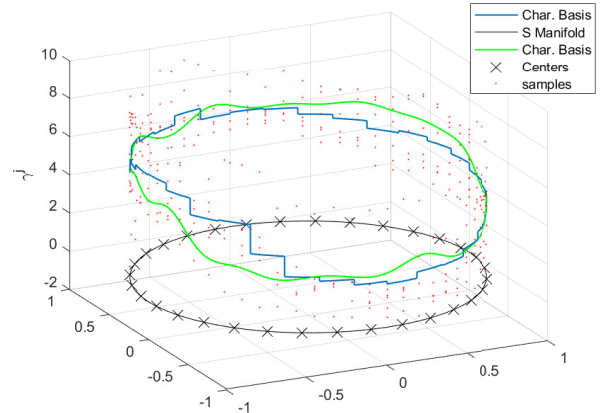


Fig. 3: Comparing two methods of approximation for a fixed number of samples, in this case 32. The blue line represents the approximation of the mapping γ^j using the partitions 1_{S_k} , while the green line represents the approximation using a kernel function basis. The low dimensional manifold S is depicted in black and the centers of each of the approximations are represented by the crosses on S . From the figure it is clear that the two methods seem to be bounded to one another.

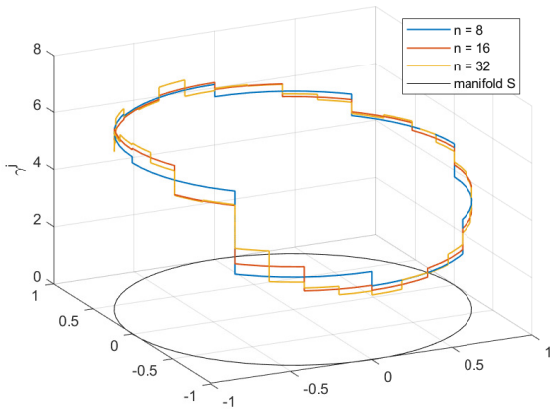
IV. FUTURE WORK

It should come as no surprise that different specimens, despite being the same species, will have some variation in the captured motion due in part to slight variations in their respective morphology. We can get a sense of this variation by comparing the motion samples collected of the elbow between gaits of two different specimens. Figure 6 depicts four gaits; two belong to one specimen and two belong to the other. Clearly, the motions can be distinguished from one another based on the specimen that produced them. Another possible contribution to the variation could be a byproduct of misaligned marker placement. From a calculation standpoint, it is difficult to see how slight variation in the placement of the markers on the back to define the body frame would lead to variation in the measured motion. Future work will aim to attempt to study these variations and seek to better control these variables.

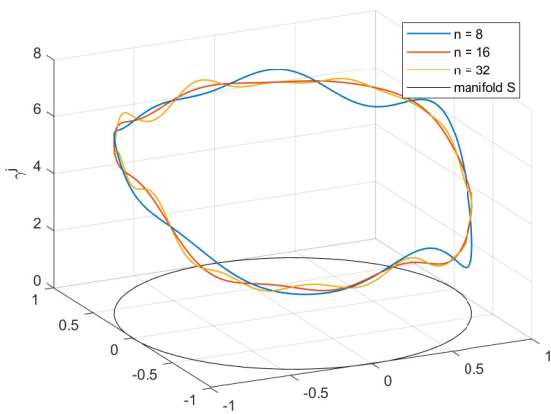
ACKNOWLEDGMENT

REFERENCES

- [1] Marc Raibert. BigDog, the rough-terrain quadruped robot. *IFAC Proceedings Volumes (IFAC-PapersOnline)*, 17(1 PART 1):6–9, 2008.
- [2] Katina Michael. Meet boston dynamics' ls3-the latest robotic war machine. 2012.
- [3] Sangok Seok, Albert Wang, Meng Yee Chuah, David Otten, Jeffrey Lang, and Sangbae Kim. Design principles for highly efficient quadrupeds and implementation on the mit cheetah robot. In *2013 IEEE International Conference on Robotics and Automation*, pages 3307–3312. IEEE, 2013.



(a)



(b)

Fig. 4: The approximations of the mapping γ^j , from (a) the partition, 1_{S_k} , basis and (b) the exponential kernel basis given a number of basis functions n . For (a) the value of the mapping over a particular partition is equivalent to the average of the samples over that partition. From the figure, it is clear that a larger number n of partitions corresponds to a higher resolution that manages to capture changes in the data over smaller intervals. Despite the differences, the approximations from both methods appear to not deviate significantly given a different number of centers.

- [4] Benjamin McInroe, Henry C Astley, Chaohui Gong, Sandy M Kawano, Perrin E Schiebel, Jennifer M Rieser, Howie Choset, Richard W Blob, and Daniel I Goldman. Tail use improves performance on soft substrates in models of early vertebrate land locomotors. *Science*, 353(6295):154–158, 2016.
- [5] Konstantinos Karakasiliotis, Robin Thandiackal, Kamilo Melo, Tomislav Horvat, Navid K Mahabadi, Stanislav Tsitkov, Jean-Marie Cabelguen, and Auke J Ijspeert. From cineradiography to biorobots: an approach for designing robots to emulate and study animal locomotion. *Journal of The Royal Society Interface*, 13(119):20151089, 2016.
- [6] Irfan Hussain, Mohammad I. Awad, Ali Bin Junaid, Federico Renda, Lakmal Seneviratne, and Dongming Gan. Dynamic modeling and numerical simulations of a passive robotic walker using Euler-Lagrange method. *11th International Symposium on Mechatronics and its Applications, ISMA 2018*, 2018-Janua(March):1–6, 2018.

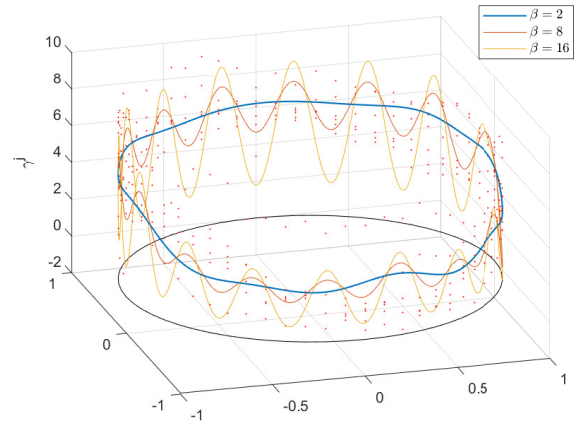


Fig. 5: The approximations using a fixed number of 16 centers for various values of the kernel hyperparameter, β . For larger values of β , the evaluation of the kernel basis quickly diminishes away from the kernel centers resulting in highly oscillatory approximations.

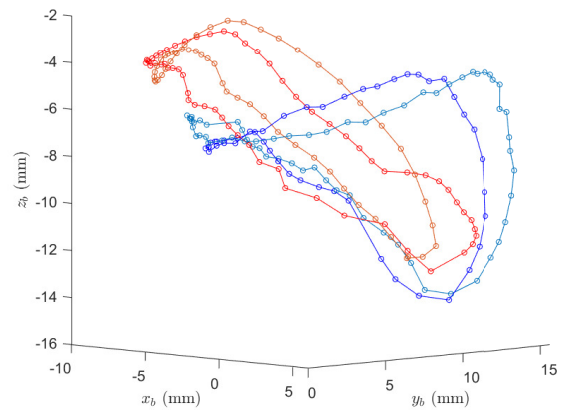


Fig. 6: The elbow motion trajectory over a number of gaits for two different specimens. Each gait is denoted by a different color. The cooler blue tones indicate one specimen while the warmer red tones indicate another. It would appear that the manifolds on which motion lies varies between specimens of the same species.

- [7] Matt J. Bender, Mark McClelland, Gerardo Bledt, Andrew Kurdila, Tomonari Furukawa, and Rolf Mueller. Trajectory Estimation of Bat Flight Using a Multi-View Camera System. *AIAA Modeling and Simulation Technologies Conference*, (January):1–13, 2015.
- [8] Rivers Ingersoll, Lukas Haizmann, and David Lentink. Biomechanics of hover performance in Neotropical hummingbirds versus bats. *Science Advances*, 4(9), 2018.
- [9] Tien Van Truong, Tuyen Quang Le, Doyoung Byun, Hoon Choel Park, and Minjun Kim. Flexible Wing Kinematics of a Free-Flying Beetle (Rhinoceros Beetle *Trypoxylus Dichotomus*). *Journal of Bionic Engineering*, 9(2):177–184, 2012.
- [10] Angela R.V. Rivera, Jeanette Wyneken, and Richard W. Blob. Forelimb kinematics and motor patterns of swimming loggerhead sea turtles (*Caretta caretta*): Are motor patterns conserved in the evolution of new locomotor strategies? *Journal of Experimental Biology*, 214(19):3314–

- 3323, 2011.
- [11] Aleksandra V. Birn-Jeffery and Timothy E. Higham. Geckos decouple fore- and hind limb kinematics in response to changes in incline. *Frontiers in Zoology*, 13(1):1–13, 2016.
 - [12] Laura B Porro, Amber J Collings, Enrico A Eberhard, Kyle P Chadwick, and Christopher T Richards. Inverse dynamic modelling of jumping in the red-legged running frog, *kassina maculata*. *Journal of Experimental Biology*, 220(10):1882–1893, 2017.
 - [13] Artur S.P. Varejão, António M. Cabrita, João A. Patrício, José Bulas-Cruz, Ronaldo C. Gabriel, Pedro Melo-Pinto, Pedro A. Couto, and Marcel F. Meek. Functional assessment of peripheral nerve recovery in the rat: Gait kinematics. *Microsurgery*, 21(8):383–388, 2001.
 - [14] Chen Li, S. Tonia Hsieh, and Daniel I. Goldman. Multi-functional foot use during running in the zebra-tailed lizard (*Callisaurus draconoides*). *Journal of Experimental Biology*, 215(18):3293–3308, 2012.
 - [15] Lei Li, James McCann, Nancy Pollard, and Christos Faloutsos. BoLeRO: A principled technique for including bone length constraints in motion capture occlusion filling. *Computer Animation 2010 - ACM SIGGRAPH / Eurographics Symposium Proceedings, SCA 2010*, pages 179–188, 2010.
 - [16] S. M. Cox and Gary B. Gillis. Forelimb kinematics during hopping and landing in toads. *Journal of Experimental Biology*, 218(19):3051–3058, 2015.
 - [17] Penny E Hudson, Sandra A Corr, and Alan M Wilson. High speed galloping in the cheetah (*acinonyx jubatus*) and the racing greyhound (*canis familiaris*): spatio-temporal and kinetic characteristics. *Journal of Experimental Biology*, 215(14):2425–2434, 2012.
 - [18] Mahmoud El-Gohary, Lars Holmstrom, Jessie Huisinga, Edward King, James McNames, and Fay Horak. Upper limb joint angle tracking with inertial sensors. *Proceedings of the Annual International Conference of the IEEE Engineering in Medicine and Biology Society, EMBS*, (October 2014):5629–5632, 2011.
 - [19] Mahmoud El-Gohary and James McNames. Shoulder and elbow joint angle tracking with inertial sensors. *IEEE Transactions on Biomedical Engineering*, 59(9):2635–2641, 2012.
 - [20] Tadashi Kashima and Keita Sugawara. Experimental and theoretical analysis of human arm trajectories in 3D movements. *Artificial Life and Robotics*, 20(3):203–209, 2015.
 - [21] Tadashi Kashima, Keita Sugawara, and Ayumi Mitoh. Kinematic properties of human arm reaching movements in a three-dimensional space. *Artificial Life and Robotics*, 23(1):41–47, 2018.
 - [22] Adam G Kirk, James F O’Brien, and David A Forsyth. Skeletal parameter estimation from optical ta. *IEEE Computer Society Conference on Computer Vision and Pattern Recognition*, pages 782–788, 2005.
 - [23] Marius CĂclin Silaghi, Ralf Plänkner, Ronan Boulic, Pascal Fua, and Daniel Thalmann. Local and global skeleton fitting techniques for optical motion capture. *Lecture Notes in Computer Science (including subseries Lecture Notes in Artificial Intelligence and Lecture Notes in Bioinformatics)*, 1537:26–40, 1998.
 - [24] Andreas Aristidou and Joan Lasenby. Real-time marker prediction and CoR estimation in optical motion capture. *User Modeling and User-Adapted Interaction*, 29(1):7–26, 2013.
 - [25] Johannes Meyer, Markus Kuderer, Jörg Müller, and Wolfram Burgard. Online marker labeling for fully automatic skeleton tracking in optical motion capture. In *2014 IEEE International Conference on Robotics and Automation (ICRA)*, pages 5652–5657. IEEE, 2014.
 - [26] Jack Wang, Aaron Hertzmann, and David J Fleet. Gaussian process dynamical models. In *Advances in neural information processing systems*, pages 1441–1448, 2006.
 - [27] Tobias Schubert, Alexis Gkogkidis, Tonio Ball, and Wolfram Burgard. Automatic initialization for skeleton tracking in optical motion capture. In *2015 IEEE International Conference on Robotics and Automation (ICRA)*, pages 734–739. IEEE, 2015.
 - [28] Xuequan Lu, Honghua Chen, Sai Kit Yeung, Zhigang Deng, and Wenzhi Chen. Unsupervised articulated skeleton extraction from point set sequences captured by a single depth camera. *32nd AAAI Conference on Artificial Intelligence, AAAI 2018*, pages 7226–7234, 2018.
 - [29] Jannik Steinbring, Christian Mandery, Nikolaus Vahrenkamp, Tamim Asfour, and Uwe D. Hanebeck. High-Accuracy Real-Time Whole-Body Human Motion Tracking Based on Constrained Nonlinear Kalman Filtering. 2015.
 - [30] Jannik Steinbring, Christian Mandery, Florian Pfaff, Florian Faion, Tamim Asfour, and Uwe D. Hanebeck. Real-time whole-body human motion tracking based on unlabeled markers. *IEEE International Conference on Multisensor Fusion and Integration for Intelligent Systems*, 0:583–590, 2016.
 - [31] Shihong Xia, Le Su, Xinyu Fei, and Han Wang. Toward accurate real-time marker labeling for live optical motion capture. *Visual Computer*, 33(6-8):993–1003, 2017.
 - [32] Dana Kulic, Gentiane Venture, Katsu Yamane, Emel Demircan, Ikuo Mizuuchi, and Katja Mombaur. Anthropomorphic Movement Analysis and Synthesis: A Survey of Methods and Applications. *IEEE Transactions on Robotics*, 32(4):776–795, 2016.
 - [33] Ross L. Hatton and Howie Choset. Geometric motion planning: The local connection, Stokes’ theorem, and the importance of coordinate choice. *International Journal of Robotics Research*, 30(8):988–1014, 2011.
 - [34] Ross L. Hatton, Yang Ding, Howie Choset, and Daniel I. Goldman. Geometric visualization of self-propulsion in a complex medium. *Physical Review Letters*, 110(7), 2013.
 - [35] Elie A. Shammass, Howie Choset, and Alfred A. Rizzi. Geometric motion planning analysis for two classes of underactuated mechanical systems. *International Journal of Robotics Research*, 26(10):1043–1073, 2007.
 - [36] Josip Česić, Vladimir Joukov, Ivan Petrović, and Dana Kulić. Full body human motion estimation on lie groups using 3D marker position measurements. *IEEE-RAS International Conference on Humanoid Robots*, pages 826–833, 2016.
 - [37] Stanislas Brossette, Adrien Escande, Grégoire Duchemin, Benjamin Chrétien, Stanislas Brossette, Adrien Escande, Grégoire Duchemin, Benjamin Chrétien, Stanislas Brossette, and Adrien Escande. Humanoid posture generation on non-Euclidean manifolds To cite this version : HAL Id : hal-01265418 Humanoid Posture Generation on non-Euclidean Manifolds. 2016.
 - [38] Stanislas Brossette, Adrien Escande, and Abderrahmane Kheddar. Multicontact Postures Computation on Manifolds. *IEEE Transactions on Robotics*, 34(5):1252–1265, 2018.
 - [39] Ahmed Shabana. *Dynamics of multibody systems*. Cambridge university press, 2020.
 - [40] Edward J Haug. *Computer aided kinematics and dynamics of mechanical systems*, volume 1. Allyn and Bacon Boston, 1989.
 - [41] Parviz E Nikravesh. *Computer-aided analysis of mechanical systems*. Prentice-Hall, Inc., 1988.
 - [42] Richard M. Murray and S. Shankar Sastry. Steering Nonholonomic Control Systems Using Sinusoids. *Nonholonomic Motion Planning*, 38(5):23–51, 1993.
 - [43] Kevin M Lynch and Frank C Park. *Modern Robotics*. Cambridge University Press, 2017.
 - [44] Francesco Bullo and Andrew D. Lewis. *Geometric Control of Mechanical Systems*, volume 49 of *Texts in Applied Mathematics*. Springer Verlag, New York-Heidelberg-Berlin, 2004.
 - [45] Darryl D Holm, Tanya Schmah, and Cristina Stoica. *Geometric mechanics and symmetry: from finite to infinite dimensions*, volume 12. Oxford University Press, 2009.
 - [46] Ralph Abraham, Jerrold E Marsden, and Tudor Ratiu. *Manifolds, tensor analysis, and applications*, volume 75. Springer Science & Business Media, 2012.
 - [47] Ronald DeVore, Gerard Kerkyacharian, Dominique Picard, and Vladimir Temlyakov. Approximation methods for supervised learning. *Foundations of Computational Mathematics*, 6(1):3–58, 2006.
 - [48] Saburo Saitoh, Daniel Alpay, Joseph A Ball, and Takeo Ohsawa. *Reproducing Kernels and Their Applications*, volume 3. Springer Science & Business Media, 2013.
 - [49] Alain Berlinet and Christine Thomas-Agnan. *Reproducing kernel Hilbert spaces in probability and statistics*. Springer Science & Business Media, 2011.
 - [50] Peter Binev, Albert Cohen, Wolfgang Dahmen, Ronald DeVore, and Vladimir Temlyakov. Universal algorithms for learning theory part i: piecewise constant functions. *Journal of Machine Learning Research*, 6(Sep):1297–1321, 2005.
 - [51] Tyson L Hedrick. Software techniques for two-and three-dimensional kinematic measurements of biological and biomimetic systems. *Bioinspiration & biomimetics*, 3(3):034001, 2008.
 - [52] Stefan Klus, Ingmar Schuster, and Krikamol Muandet. Eigendecompositions of transfer operators in reproducing kernel hilbert spaces. *Nonlinear Science*, 30:283–315.
 - [53] Andrew J Kurdila and Parag Bobade. Koopman theory and linear approximation spaces. *arXiv preprint arXiv:1811.10809*, 2018.